Optimizing electrochemical micromachining parameters for Zr-based bulk metallic glass

K.M. Cole [a],[*], D.W. Kirk [b], C.V. Singh [a], S.J. Thorpe [a]

[a] Department of Materials Science and Engineering, University of Toronto, 184 College St., Toronto, Ontario M5S3E4, Canada
[b] Department of Chemical Engineering and Applied Chemistry, University of Toronto, 200 College St., Toronto, Ontario M5S3E4, Canada

ABSTRACT

Bulk metallic glasses (BMGs) contain a unique combination of enhanced mechanical and chemical properties due to the absence of crystalline features, but their machining processes are still being developed. Electrochemical micromachining (ECMM) with microtool electrodes is a promising technique for microshaping BMGs without the use of elevated temperatures or deformation – both of which can induce crystallization. This work systematically studied the mechanisms and processing parameters responsible for degradation of the material surface allowing the development of a novel protocol for utilizing the ECCM technique for Zr based BMGs. Anodic polarization of $Zr_{57}Ni_{20}Al_{15}Cu_{5.5}Nb_{2.5}$ BMGs in 2.94 M $NaNO_3$ and subsequent microscopy revealed that the primary corrosion mechanism during electrochemical micromachining is pitting. Through chronoamperometry the repassivation potential was determined to be 2.235 V. This voltage was used to prevent spontaneous repassivation during electrochemical micromachining. The Taguchi method was used to assess the effect of electrolyte flow rate, duty cycle and pulsed voltage range. Signal-noise ratios and analysis of variance were used to optimize ECMM parameters of the electrochemical micromachining process. Through this method, an electrolyte flow rate of 0.4 L/min with a duty cycle of 1:10 and a voltage range of 2.235–3 V was determined to yield the optimal holes with respect to the aspect ratio, surface roughness and the rate of electrochemical micromachining of Zr-based BMGs.

© 2016 The Society of Manufacturing Engineers. Published by Elsevier Ltd. All rights reserved.

1. Introduction

The unique combination of enhanced mechanical and chemical properties which bulk metallic glasses (BMGs) possess are derived from their amorphous structure [1,2]. In particular, their high strength and hardness make them attractive choices as structural materials in microelectromechanical systems (MEMS) [3,4]. These small components are typically fabricated through thermomechanical processing in the supercooled liquid region [5]. For materials which do not possess a large supercooled liquid region, other means of machining which would not induce crystallization at room temperature are required.

Electrochemical micromachining (ECMM) is a rapidly developing technique which allows for microshaping of the surface at room temperatures [6–9]. It has been used in a wide range of applications, particularly in the fabrication of circuit boards [10]. This technique works by taking a fine tip cathode (i.e. Pt) in an electrolyte and bringing it to within a few microns of the anode (i.e. BMG surface) while pulsing a voltage. A pulsing voltage causes localized anodic dissolution and can produce very fine localized machining. For a stationary tool, the size and shape of the machined hole is related to the shape of the cathode, the distance between it and the anode, and the electrolyte composition/conductivity [11]. While ECMM has been demonstrated on a wide range of crystalline materials, it is much more challenging when applying to metallic glasses due to their high chemical resistance [11–13].

Recently it has been shown by Horn et al. [14] that ECMM can successfully electrochemically micromachine Fe-based BMGs. A systematic approach showed the effects of varying pulse-on times and peak voltages during the machining process. While these results were promising, an effective ECMM process for Zr-based BMGs in aqueous solutions has not yet been developed due to their ability to spontaneous passivate. This spontaneous passivation often causes dense corrosion products and oxides to adhere to the surface which prevent further machining. With regards to Zr-based BMGs, Koza et al. [11] were able to perform ECMM when using a methanolic $HClO_4$ solution; however, the most commonly used ECMM electrolytes in industry are aqueous based solutions

* Corresponding author.
  E-mail address: kevin.cole@mail.utoronto.ca (K.M. Cole).

due to their relative ease in preparation and safety compared to organic electrolytes [6]. In particular, the preferred electrolyte is sodium nitrate ($NaNO_3$) as this electrolyte offers many advantages over other electrolytes in terms of having a low throwing power, and rapid and precise metal removal that lead to faster machining times [6,15].

Previous attempts to electrochemically micromachine Zr-based BMGs reported $NaNO_3$ unsuitable due to the formation of these thick and dense corrosion product layers which adhered to the surface [11]. This suggests that adequate removal of these corrosion products is essential for electrochemically machining Zr-based BMGs in aqueous solutions. Parameters such as electrolyte flow rate, duty cycle and voltage range, along with peak voltage and pulse-on time can be carefully chosen to aid in the removal or prevention of corrosion products from adhering to the surface. Understanding the role of these parameters will allow for optimization of the ECMM process which is lacking for a large class of BMG materials.

In the present study, the effect of electrolyte flow rate, duty cycle, and voltage range was investigated to improve the machining process on $Zr_{57}Ni_{20}Al_{15}Cu_{5.5}Nb_{2.5}$. This alloy was previously shown to only have a moderate supercooled liquid region and therefore required processing techniques at room temperature, such as ECMM, to produce MEMS devices [16,17]. Experiments were designed using the Taguchi method of an orthogonal array to assess the effect of each of these parameters [18]. Through these experiments, it was shown that ECMM can be successfully performed on Zr-based BMGs through optimization of the electrochemical micromachining parameters. A new method of using a base voltage during pulse-off time is presented which reduces corrosion product adhesion to the surface to enhance the machining of Zr-based BMGs.

2. Experimental

2.1. Sample preparation and surface finish

Ingots with nominal compositions of $Zr_{57}Ni_{20}Al_{15}Cu_{5.5}Nb_{2.5}$ were prepared through arc melting and suction casting into a copper mold. The metals, in the form of slugs, Zr (99.95 wt.%), Ni (99.98 wt.%), Al (99.999 wt.%), Cu (99.995 wt.%) and Nb (99.95 wt.%) were weighed using a Mettler AE260 balance before being placed in the arc melter (Edmund Bühler Compact Arc Melter MAM-1). Before melting, the caster was pumped down to approximately 0.1 mbar using a roughing pump and then filled back to atmospheric pressure using high purity argon (99.9999%). This step was repeated five times for each sample to ensure the oxygen content remained consistent. Each ingot was then melted four times for 15 s under high purity argon. Between each melting step, the ingot was flipped to achieve improved chemical homogeneity before being finally suction cast after the fourth melting cycle. Further details can be found in Ref. [14].

Rod samples were prepared with a diameter of 3 mm and a length of 30 mm, and were sectioned using a diamond blade cutter for testing. This diameter was chosen for investigation such that it would comply with all required testing equipment. Samples were embedded in epoxy resin and progressively ground on 400, 600, and 1200 grit SiC paper. For imaging, samples were polished to a final surface finish of 1 μm using diamond paste. Transmission electron microscopy (TEM) samples were produced using focus ion beam milling with a gallium beam at 5 kV. X-ray diffraction (XRD) with Cu K_α was used to analyze the structure of the rods from 20 to 80° at a scan speed of 6 s per 0.03° step size (Rigaku Miniflex 600). The rods were imaged and inspected for crystals using high resolution scanning electron microscopy (SEM, Hitachi SU3500) and
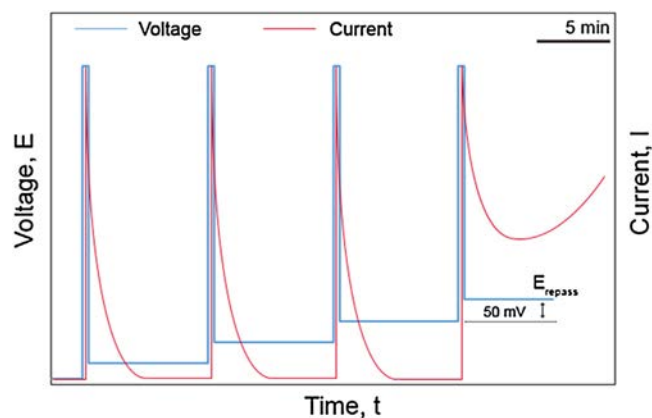
Fig. 1. Schematic showing current response with voltage pulsing during chronoamperometry experiments. The base voltage was increased by 50 mV after every pulse to produce a voltage staircase. E_{repass} was defined as the potential at which the current was observed to increase while holding the potential constant at a given base voltage.

TEM (FEI Titan 80-300 LB). Selected area diffraction (SAD) patterns were produced during TEM at 300 kV to confirm the structure was amorphous. Energy-dispersive X-ray spectroscopy (EDX) was used at 20 kV during SEM to determine as-cast compositions. Topology of machined surfaces was analyzed using white light profilometry (Zygo Newview 100).

2.2. Electrochemical analysis

For electrochemical testing and machining, BMG samples were embedded in epoxy resin and progressively ground on 400, 600, and 1200 grit SiC paper. A copper wire was attached to the BMG surface using silver paint to produce a working electrode. Samples were masked using Amercoat 90HS® to prevent crevice corrosion at the epoxy/BMG interface. Deionized water and ethanol were used to clean the BMG surface before electrochemical testing and machining. Anodic polarization was performed to determine the electrochemical behavior of $Zr_{57}Ni_{20}Al_{15}Cu_{5.5}Nb_{2.5}$ BMGs in 2.94 M $NaNO_3$ solution (Ivium Stat). Solutions were prepared using Type I water and analytical grade $NaNO_3$ (>99%). Polarization was conducted using a three electrode setup with a platinum mesh as the counter electrode, the BMG as the working electrode and an Ag/AgCl reference electrode. Samples were immersed in electrolyte for 30 min to achieve a stable open cell potential (OCP) prior to subsequent measurements. Scans were produced by sweeping voltage at 1 mV/s between −0.9 to 3.5 V vs. Ag/AgCl. Polarization tests were repeated at least three times to ensure reproducibility.

Chronoamperometry was utilized to determine the repassivation potential (E_{repass}) using the same three electrode apparatus. Tests were conducted in a step wise staircase fashion as shown schematically in Fig. 1. The voltage was pulsed to 3 V and held for a period of 5 s, and then pulsed back to a base voltage while monitoring the current in each step. With each subsequent pulse to 3 V, the base voltage was increased in 50 mV steps. E_{repass} was determined to be the voltage at which the corresponding current no longer returned to zero.

Electrochemical micromachining experiments were performed using the electrochemical apparatus shown in Fig. 2. The electrochemical cell with a BMG sample was mounted on a Newport 2-axis tilt stage to level and reduce vibrations while machining. Once the sample was leveled, the 10 μm diameter counter electrode (CH Instruments) was positioned within 1–5 ± 0.5 μm of the surface using an x-y-z motorized stage (Zaber Tech T-LSM050A). The position of the tool tip was determined by bringing the tool tip lightly into contact with the BMG surface and then raised a defined
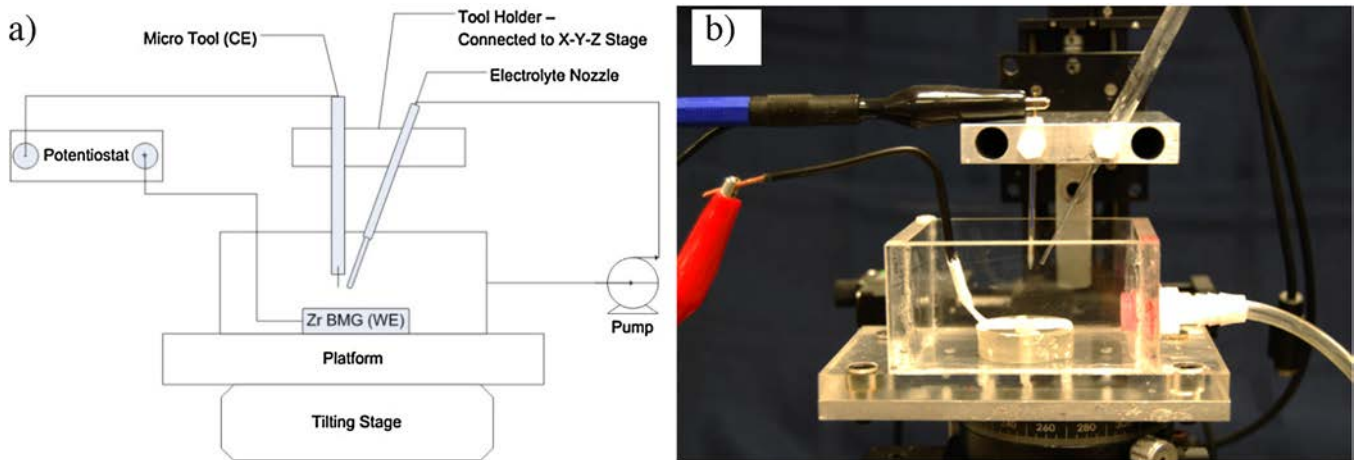
Fig. 2. ECMM cell setup used for machining of $Zr_{57}Ni_{20}Al_{15}Cu_{5.5}Nb_{2.5}$ BMGs. (a) Schematic of ECMM setup with auxiliary components used during machining. (b) Photo of apparatus before machining. Counter electrode is a 10 μm Pt tool encapsulated in glass and working electrode is a copper wire attached to BMG using silver paint.

distance using the motorized stage. Electrolyte was then added (~150 mL) and the BMG was left immersed for 30 min to obtain an accurate measurement of the open circuit potential prior to electrochemical micromachining. Circulation of the electrolyte was controlled using a pulseless variable flow chemical pump (Fisher Scientific). The DC voltage was provided using the pulse generator mode within the Ivium Stat.

3. Results and discussion

3.1. Structural characterization and electrochemical behavior

Amorphous structures were verified using high resolution TEM imaging and selected area diffraction as seen in Fig. 3. No evidence of crystallization was present in bright or dark field images. Only broad diffuse rings were observed in diffraction confirming the as-cast structure was fully amorphous. The electrochemical behavior of Zr-based BMG samples in aerated 2.98 M $NaNO_3$ at room temperature was tested prior to machining and used to determine pulsing parameters as shown in Fig. 4 for the anodic polarization curve of $Zr_{57}Ni_{20}Al_{15}Cu_{5.5}Nb_{2.5}$. Fig. 4 is divided into four regions which indicate transitions that are observed during anodic polarization. As the potential was increased to around 0.2 V (region I), the sample spontaneously passivated. The presence of Nb and the lack of crystalline defects made it easy to passivate as noted by the absence of a

Tafel slope on the anodic side and steady current densities throughout the region. At voltages around 1.1–1.6 V (region II) there was a gradual increase in current that can be attributed to the onset of the oxygen evolution reaction. The emergence of another (secondary) passive layer in region III has been previously noted to correspond to a change in higher oxidation states within the passive film [19]. A sharp increase in current around 2.1 V is noted as the breakdown potential (E_b) and the onset of a mass transport regime as noted by the current plateau. Analyzing the surface with SEM after anodic polarization showed signs of pitting which is consistent with other Zr-based BMGs [11].

Since pitting is the primary mechanism for removal of material, it is also important to understand the electrochemical behavior when a high voltage is pulsed to produce a pit and then removed. To evaluate this, chronoamperometry was performed and the corresponding current was observed. Fig. 5 shows the current profiles for voltage ranges of 0–3 V, 1.785–3 V, and 2.235–3 V. The sharp increase in current arises from the nucleation and stable pit growth. Once the potential is removed and the sample is able to repassivate, the current dropped back to the OCP current and stabilized, as seen in Fig. 5 for 0–3 V. It was noted that when a base voltage of 1.785 V was used, the current did not immediately return to its initial value. It is believed that this potential corresponded to the transpassive behavior of oxides formed during secondary passivity. Continuing to increase the base voltage with subsequent pulses showed the
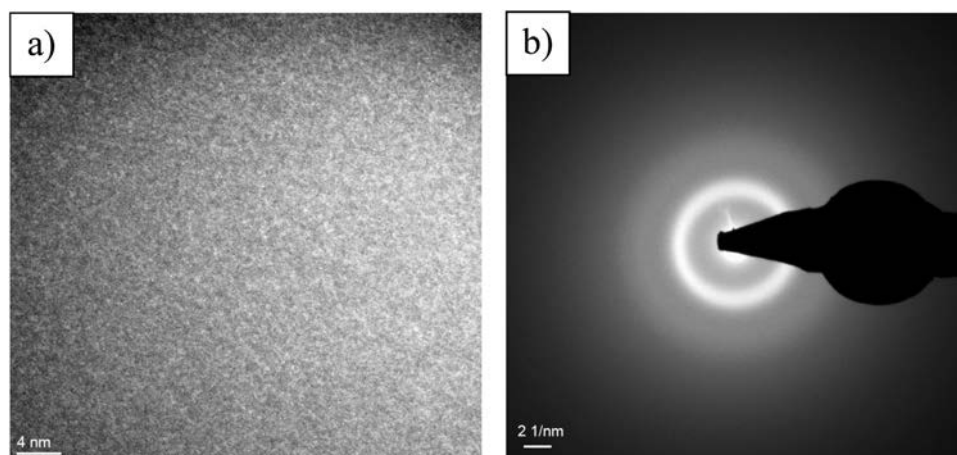
Fig. 3. TEM images for verification of amorphous structure. (a) High resolution bright field TEM image showing no second phase crystals and only diffuse contrast, and (b) selected area diffraction pattern showing only broad diffused rings.
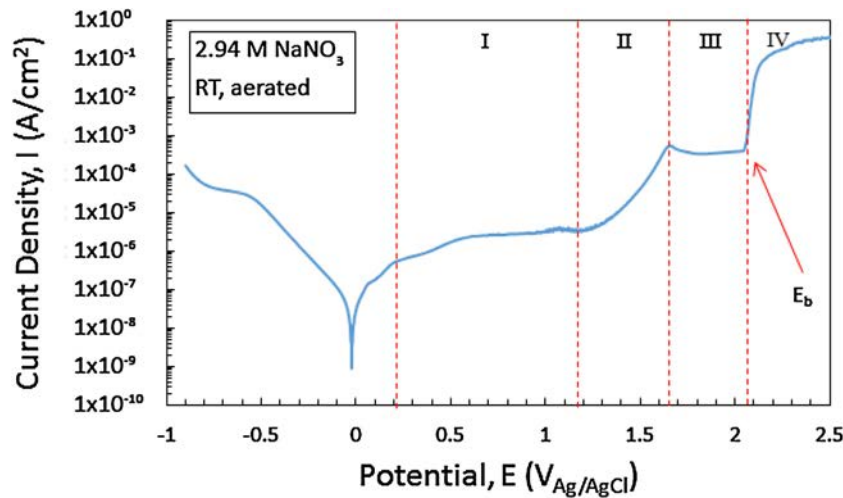
Fig. 4. Anodic polarization scan for $Zr_{57}Ni_{20}Al_{15}Cu_{5.5}Nb_{2.5}$ in 2.94 M NaNO$_3$ at room temperature and open air with scan rate of 1 mV/s. Section I is the passive region, II is the O$_2$ reaction, III is a change is oxidation states and IV is the pitting region.

repassivation potential (E_{repass}) to be 2.235 V since the current continued to increase with time. Comparing these values to those seen during anodic polarization in Fig. 4 for the transition from region II to III and III to IV showed a slight shift to the right. This shift on the reverse scan further verified that pitting is the primary electrochemical machining mechanism in Zr-based BMGs. These values were then used during the machining process in order to reduce or eliminate oxide layers from forming on the surface. Additionally, the slight difference in E_b and E_{repass} is important for understanding the overpotential that is actually being applied and ensuring a sufficient bias to prevent redeposition of metal ions and corrosion products onto the surface.

3.2. Electrochemical machining process

The main hindrance for performing ECMM on Zr-based BMGs in NaNO$_3$ is the formation of corrosion products on the surface. Therefore, the parameters selected for our investigation focused on removing or preventing corrosion products from adhering to the surface during ECMM. These parameters included duty cycle (pulse

on time: pulse off time), voltage range (base and peak voltage), and electrolyte flow rate and their interdependence.

The time constant for charging and discharging the double layer can be estimated through the following equation: $\tau = C_{DL} \times d \times \rho$ [12]. This equation shows that the time constant (τ) is the product of the double layer capacitance (C_{DL}), the distance between the surface and electrode (d) and the resistivity of the electrolyte (ρ). Through cyclic voltammetry in the non-Faradic region (± 0.1 V from OCP) it was determined that the double layer capacitance for this material was approximately 25 μF/cm^2 and was consistent with literature values. Therefore, by varying the distance between the tool tip and the sample, two different regimes of machining can be investigated. When operating in the range of 1–5 μm and using 25 wt.% NaNO$_3$ ($\rho = 0.8$ Ωm), the time constant for charging and discharging the double layer is between 0.2–1 μs. However, when the distance is increased to a more conventional electrochemical micromachining working distance of 50 μm, the time constant becomes 10 μs.

In the former case, the pulse duration used in this study (10 μs) are much greater than that for double layer charging, while in the latter case the pulse duration is of the same order of magnitude.
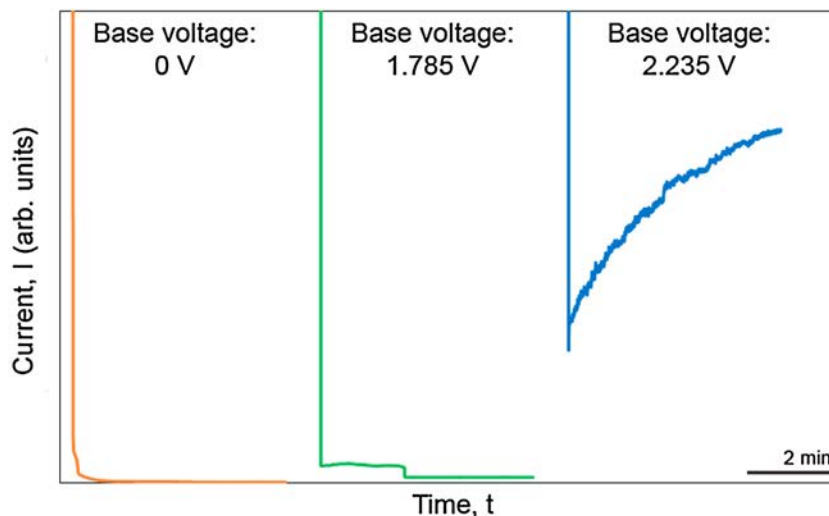
Fig. 5. Current vs. time responses when applying a voltage of 3 V during chronoamperometry experiments with various base voltages. Base voltage of 0 V shows typical current vs. time response when pulsing voltage. At 1.785 V the current does not immediately return to zero. For base voltage of 2.235 V the current never returns to zero and stabilizes indicating E_{repass}.
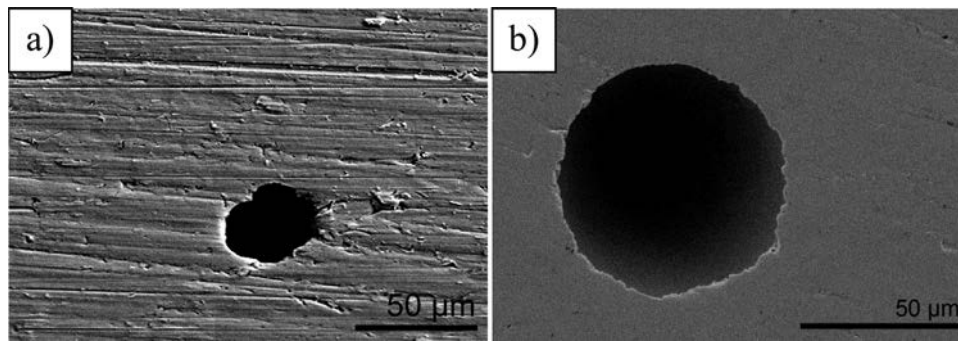
Fig. 6. SEM image of hole produced using pulse range of 2.235–3 V, duty cycle of 1:10, and pulse on of 10 μs for (a) working distance of 5 μm and (b) working distance of 50 μm.

Initial electrochemical testing was performed at a variable working distance of 5 and 50 μm to note the effect of ECMM in each regime as shown in Fig. 6. When the pulse time is much longer than the time constant, small, slightly asymmetric holes were produced (Fig. 6a). By comparison much bigger symmetric holes were produced when the pulse time was of the same order as the time constant as shown in Fig. 6b.

Additional initial ECMM screening tests were conducted to study the effect of flow at a constant working distance of 50 μm as shown in Fig. 7. The presence of flow was beneficial to the uniformity of ECMM as seen in comparing Fig. 7a and b. While in many cases electrolyte flow is not ideal for ECMM, it can be seen that it is necessary for proper machining. Sodium nitrate is a passivating electrolyte which contains large oxidizing anions which allows fast machining rates but also creates corrosion products which adhere to the surface. The presence of electrolyte flow aids in the removal of these corrosion products which means $NaNO_3$ only has to conduct electric current to the surface for removal of material. A concentration of 2.94 M $NaNO_3$ is slightly acidic which helps to remove reaction products.

3.3. Optimization of electrochemical micromachining

The previous initial ECMM results have demonstrated that electrochemical machining is possible on Zr-based BMGs using aqueous $NaNO_3$ for both electrochemical machining regions with the presence of electrolyte flow and appropriate waveform.

To further investigate the electrochemical micromachining process, the machining parameters were investigated in detail within the near micron region (d ≤ 5 μm). Table 1 lists these parameters and their ranges evaluated in this study. Duty cycle is not only important for the resolution obtained during machining but also gives time for corrosion products to be swept away. Voltage ranges were determined from the previous electrochemical testing noted above. From anodic polarization scans, it was determined that the peak voltages needed to be higher than 2.1 V for pitting to occur. Additionally, the rate of machining was observed to be largely affected by the peak voltage during the *on* time. Base voltages were

chosen based on chronoamperometry measurements as shown in Fig. 5.

The effect of ECMM parameters was investigated by conducting matrix experiments using the Taguchi's orthogonal array [18]. Herein, there are four different parameters with three different levels so that an L_9 orthogonal array was selected. This leads to nine experiments which could be performed and analyzed to determine the optimal machining parameters for improving aspect ratio, surface roughness and hole depth within these parameter ranges. The parameters for each of these experiments can be viewed in Table 2.

After performing each of the experiments in Table 2, the aspect ratio, the roughness within holes, and the depth of holes was tabulated and is presented in Table 3. The corresponding SEM images can be viewed in Fig. 8 along with the corresponding parameters used. Duplicates of each sample were prepared to generate an error range for the aspect ratio. Errors associated with surface roughness and depths are given by the root mean squared (RMS) value and are summarized in Table 3.

To analyze the results generated from the L_9 in further detail, signal-to-noise (S/N) ratio and ANOVA (analysis of variance) were performed. The S/N ratios (η) were measured according to the following equation:

$$\eta = -10log\left[\frac{1}{n}\sum_{i=1}^{n}\frac{1}{y_i^2}\right]$$

where n is the number of experiments and y_i represent observations of the quality characteristics under different noise conditions. This type of S/N ratio is referred to as a larger-the-better-type, whereby the larger S/N ratios provide better response. The S/N ratios were determined for the nine experiments in the Taguchi L_9 (Table 2) for each of the different parameters. Fig. 9 shows the mean S/N ratio values for how different levels of each parameter affect the performance criteria of improving aspect ratio, roughness, and depth. These plots aid in determining the quality of each value when trying to determine their effect on performance criteria.

Table 1
ECMM parameters and levels used to test and assess machining efficiency on $Zr_{57}Ni_{20}Al_{15}Cu_{5.5}Nb_{2.5}$ BMGs.

Parameters	Levels		
	1	2	3
A: peak voltage (V)	3	4	5
B: duty cycle (t_{on}:t_{off})	1:1	1:5	1:10
C: flow rate (L/min)	0.2	0.3	0.4
D: base voltage (V)	0	1.785	2.235

Table 2
ECMM experiments for optimizing machining parameters according to Taguchi's orthogonal array.

Experiment number	A (V_{peak})	B (t_{on}:t_{off})	C (L/min)	D (V_{base})
1	3	1:1	0.2	0
2	3	1:5	0.3	1.785
3	3	1:10	0.4	2.235
4	4	1:1	0.3	2.235
5	4	1:5	0.4	0
6	4	1:10	0.2	1.785
7	5	1:1	0.4	1.785
8	5	1:5	0.2	2.235
9	5	1:10	0.3	0
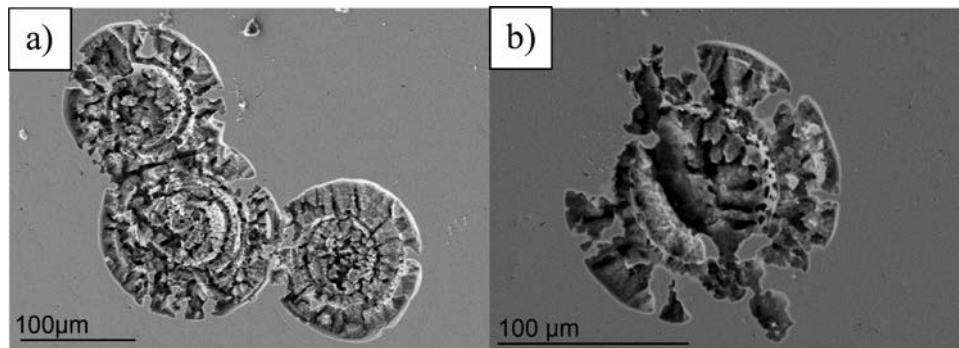
Fig. 7. SEM images comparing the machining using 0–3 V range and 1:10 duty cycle with (a) electrolyte flow of 0.4 L/min and (b) no electrolyte flow.

Table 3
List of aspect ratios, surface roughness, depth, RMS and comments for ECMM holes.

	Experiment #	Aspect ratio	Ra (μm)	Depth (μm)	RMS	Shape factor
3 V Sample	1	1.41 ± 0.17	0.77	2.478	0.9	Irregular
	2	1.25 ± 0.18	1.658	6.281	1.65	Stepped-circular
	3	1.29 ± 0.07	0.091	11.063	0.109	Circular
4 V Sample	4	1.44 ± 0.31	0.378	1.278	0.422	Irregular
	5	1.59 ± 0.58	0.592	2.034	0.635	Oval
	6	1.63 ± 0.37	0.308	1.264	0.35	Oval
5 V Sample	7	1.04 ± 0.20	0.134	1.074	0.218	Irregular
	8	1.32 ± 0.21	0.118	0.811	0.166	Stepped-oval
	9	1.37 ± 0.30	0.099	1.167	0.179	Oval

Table 4 lists the key levels for each parameter to enhance the individual performance criteria based on S/N ratios. While S/N ratios are valuable in determining the quality of signals, further optimization and impact analysis can be performed through ANOVA.

By performing ANOVA on the S/N ratios derived from Taguchi experiments, the significance of the individual control factors and their interactions can be determined. This information is important for assessing which parameters have a key impact on each of the design criteria. Table 5 summarizes the ANOVA results with each of the parameters having a degree of freedom equal to 2 and a critical F-value (F_{crit}) of 5.14. The sum of squares (S.S.) gives information of the variance of each parameter on different criteria. Method of least squares (M.S.) is also applied to determine the error of variance and is equal to the minimum value of the sums of squares about some reference value divided by the degrees of freedom for error. The F-value is the most critical parameter as it gives information of the significance of each parameter. Any F-value close to or greater than the F_{crit} is deemed to have a significant effect on the performance.

3 V Set:
(1) 0 V, 1:1, 0.2 L/min
(2) 1.785 V, 1:5, 0.3 L/min
(3) 2.235 V, 1:10, 0.4 L/min

4V Set:
(4) 2.235 V, 1:1, 0.3 L/min
(5) 0 V, 1:5, 0.4 L/min
(6) 1.785 V, 1:10, 0.2 L/min

5V Set:
(7) 1.785 V, 1:1, 0.4 L/min
(8) 2.235 V, 1:5, 0.2 L/min
(9) 0 V, 1:10, 0.3 L/min
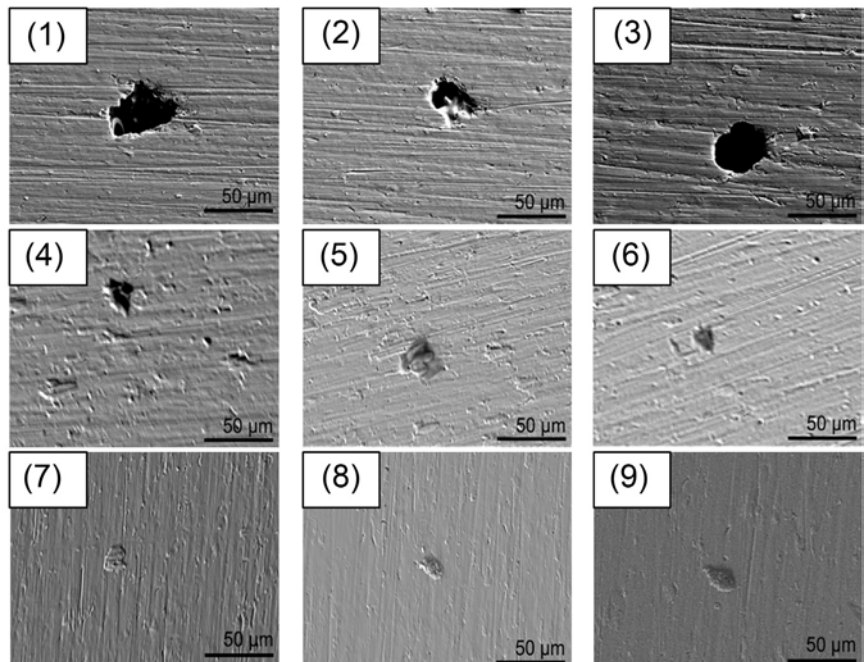
Fig. 8. SEM micrographs for ECMM holes made in $Zr_{57}Ni_{20}Al_{15}Cu_{5.5}Nb_{2.5}$ BMGs using aerated 2.98 M $NaNO_3$ at room temperature. Numbers correspond to experiment number in Table 2.
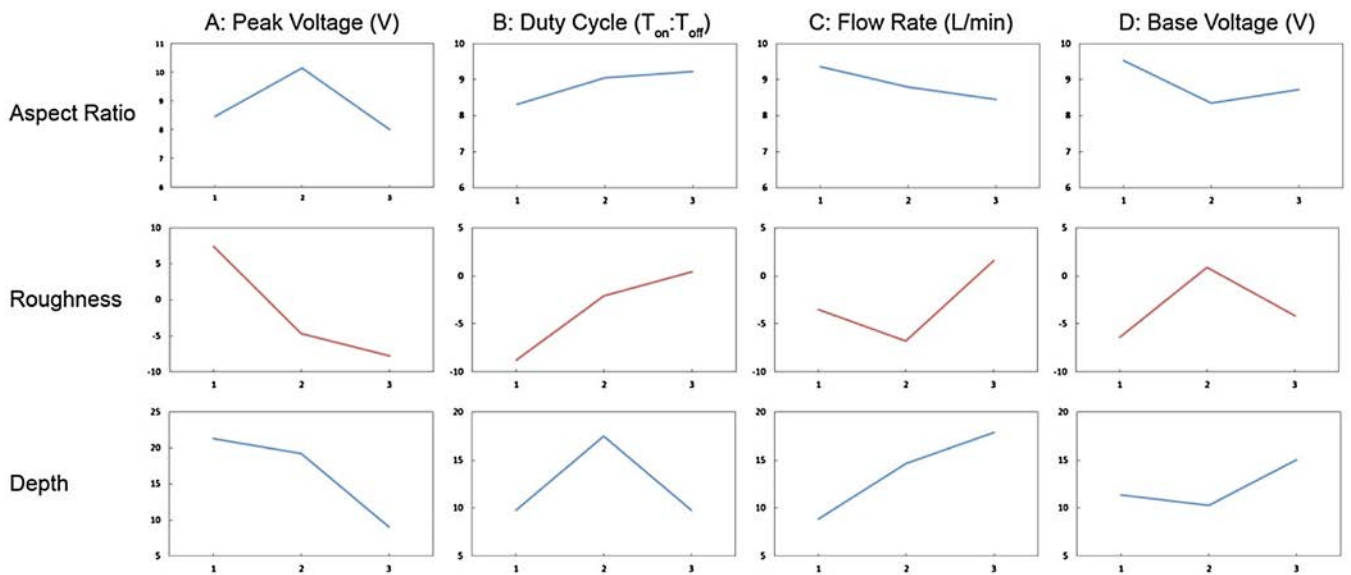
Fig. 9. Mean S/N ratio plots for each parameter vs. level on the various performance criteria (aspect ratio, roughness, and depth). A – Peak voltage, B – duty cycle, C – flow rate, and D – base voltage.

Table 4
Ideal levels for each parameter to improve individual machining criteria based on S/N ratios.

	Aspect ratio	Roughness	Depth
A: peak voltage	2	1	1
B: duty cycle	3	3	2
C: flow rate	1	3	3
D: base voltage	1	2	3

After analyzing the results from the ANOVA results it can be seen that the peak voltage has the greatest impact on the aspect ratio, roughness and depth of the holes. Referring back to Fig. 9 also gives information about which peak voltage provides the best resolution (i.e. 4 V for aspect ratio and 3 V for roughness and depth).

Each set of experiments (i.e. 3 V, 4 V, and 5 V) was performed on separate samples to study the effects of peak voltage individually among the other parameters. The use of different samples may have lead to slight differences in the exact working distance between samples; however, due to the low resistivity of the electrolyte (0.8 Ωm) the change in solution resistance under the tip could be neglected. Results generated from S/N ratios and ANOVA tables show slightly different optimal parameters based on the individual design criteria. For example, a high flow rate of 0.4 L/min was shown to be good for achieving low roughness and large depths, but a low flow rate of 0.2 L/min was seen to be desirable for an optimal aspect ratio since the jet would cause variations. Even though the ANOVA F-values showed peak voltage as having the most significant impact, the other parameters still play crucial roles in the machining process but the difference in levels do not have a

significant impact. This impact from peak voltage has been noted in previous work since too high of a voltage can cause severe pitting to occur producing rough surfaces [14,19].

Overall, the best combination of aspect ratio, roughness and depth was found to have a voltage range of 2.235–3 V with 1:10 duty cycle and 0.4 L/min flow rate. These parameters can be seen in experiment 3, and by visual inspection of the hole produced in Fig. 8 provides experimental support. These parameters were then used to test the feasibility of producing lines on a surface in attempt to be able to pattern a larger area. Fig. 10 shows a line produced using these parameters at a movement speed of 0.5 μm/s. The depths of these lines are not very deep and can be attributed to the somewhat fast movement speed and slow pulsing. Previous work by Horn et al. [14] had shown production of complex shapes in Fe-based BMGs using a movement speed of 0.1 μm/s, which is significantly slower than that in our study. Pairing this with their use of nano pulses, the features seen here are not as refined. Nonetheless, Fig. 10 does show there is a good dimensional tolerance and accuracy associated with this technique. Faster pulsing and slower movement speeds would further increase the electrochemical machining process in Zr-based BMGs.

Table 5
ANOVA table from S/N ratios showing the sums of squares (S.S.), method of least squares (M.S.), and F-value. For each parameter the degree of freedom was 2 and an F_{crit} of 5.14.

	Aspect ratio			Roughness			Depth		
	S.S.	M.S.	F-value	S.S.	M.S.	F-value	S.S.	M.S.	F-value
A	7.70	3.85	4.73	190.51	95.26	1.68	383.06	191.53	11.61
B	1.39	0.69	0.37	158.56	79.28	1.28	31.46	15.73	0.21
C	1.27	0.64	0.34	58.82	29.41	0.37	62.74	31.37	0.45
D	2.22	1.11	0.64	122.66	61.33	0.90	4.77	2.39	0.03

Fig. 10. SEM secondary electron image of ECMM lines produced using experiment 3 parameters at 0.5 μm/s in 2.94 M NaNO3. Main image is zoomed in portion of line seeing in bottom left corner.

4. Conclusions

The electrochemical behavior of $Zr_{57}Ni_{20}Al_{15}Cu_{5.5}Nb_{2.5}$ in aqueous 2.98 M $NaNO_3$ was studied through anodic polarization and chronoamperometry. The results demonstrated that the primary mechanism for material removal is pitting. Chronoamperometry revealed 2.235 V to be the repassivation potential for this alloy. Utilizing a combination of voltage thresholds/regimes for pitting and repassivation, a novel waveform was designed to effectively reduce corrosion products and dense oxides from adhering to the surface which had previously hindered ECMM of Zr-based BMGs ineffective in aqueous electrolytes while electrochemically micromaching in a potential range for anodic dissolution via pitting.

The ECMM process on Zr-based material was conducted through a series of experiments according to Taguchi's L_9 matrix. Optimum parameters were determined though S/N ratios and ANOVA. Through these experiments it was seen that successful ECMM was achieved on Zr-based BMG in aqueous solution. Analyzing the results showed the use of a 2.235 V base voltage led to holes with good aspect ratio. Additionally, the use of high flow rates to remove any corrosion products fostered greater depths while larger duty cycles produced smoother surfaces. Each of these parameters was noted to significantly affect different aspects of the machining process. The optimal machining parameters were determined to have a voltage range of 2.235–3 V, 1:10 duty cycle, and 0.4 L/min flow rate. Using these parameters allowed for the smoothest surface finish, greatest depth and best dimensional tolerance.

Lines were patterned onto the surface using the optimal ECMM parameters. These findings demonstrate that ECMM is a viable technique for micromachining Zr-based BMGs in aqueous electrolyte. This result will allow for fast and effective machining Zr-based BMGs in industry. Lines could be further enhanced through the use of shorter pulse times and slower movement speeds to produce more complex shapes and parts.

Acknowledgements

References

[1] Inoue A. Stabilization of metallic supercooled liquid and bulk amorphous alloys. Acta Mater 2000;48(1):279–306.
[2] Johnson WL. Bulk glass-forming metallic alloys: science and technology. MRS Bull 1999;24(10):42–56.
[3] Greer AL, Ma E. Bulk metallic glasses: at the cutting edge of metals research. MRS Bull 2007;32(8):611–9.
[4] Schroers J, Nguyen T, O'Keeffe S, Desai A. Thermoplastic forming of bulk metallic glass—applications for MEMS and microstructure fabrication. Mater Sci Eng: A 2007;449–451:898–902.
[5] Kumar G, Desai A, Schroers J. Bulk metallic glass: the smaller the better. Adv Mater 2011;23:461–76.
[6] Sen M, Shan HS. A review of electrochemical macro- to micro-hole drilling processes. Int J Mach Tools Manuf 2005;45:137–52.
[7] Bhattacharyya B, Munda J, Malapati M. Advancement in electrochemical micromachining. Int J Mach Tools Manuf 2004;44:1577–89.
[8] Sueptitz R, Horn S, Stoica M, Uhlemann M, Gebert A. Electrochemical micromachining of passive electrodes—application to bulk metallic glass. J Mater Process Technol 2015;219:193–8.
[9] Singh S, Jain VK, Choudhury SK. Quality aspects of electrochemical micro drilling with insulated tool and masked workpiece. In: International mechanical engineering congress and exposition. 2013.
[10] Singh J, Jain VK, Ramkumar J. Fabrication of complex circuit on printed circuit board (PCB) using electrochemical micromachining. Int J Adv Manuf Technol 2016;85(9):2073–81.
[11] Koza JA, Sueptitz R, Uhlemann M, Schultz L, Gebert A. Electrochemical micromachining of a Zr-based bulk metallic glass using micro-tool electrode technique. Intermetallics 2011;19:437–44.
[12] Schuster R, Kirchner VV, Allongue P, Ertl G. Electrochemical micromachining. Science 2000;289:98–101.
[13] Kock M, Kirchner V, Schuster R. Electrochemical micromachining with ultrashort voltage pulses—a versatile method with lithographical precision. Electrochim Acta 2003;48:3213–9.
[14] Horn S, Oswald S, Stoica M, Uhlemann M, Gebert A. Complex microshaping of bulk metallic glass surfaces by electrochemical means. J Mater Res 2015;30(22):3493–501.
[15] Bejar MA, Eterovich F. Wire-electrochemical cutting with a $NaNO_3$ electrolyte. Int J Mater Process Technol 1995;55:417–20.
[16] Cole KM, Kirk DW, Singh CV, Thorpe SJ. Role of niobium and oxygen concentration on glass forming ability and crystallization behavior of Zr–Ni–Al–Cu–Nb bulk metallic glasses with low copper concentration. J Non-Cryst Solids 2016;445–446:88–94.
[17] Li Y, Zhang W, Qin F, Makino A. Mechanical properties and corrosion resistance of a new $Zr_{56}Ni_{20}Al_{15}Nb_4Cu_5$ bulk metallic glass with a diameter up to 25 mm. J Alloys Compd 2014;615:571–4.
[18] Phadke MS. Quality engineering using robust design. Englewood Cliffs, NJ: Prentice-Hall; 1989.
[19] Gebert A, Gostin PF, Sueptitz R, Oswald S, Abdi S, Uhlemann M, Eckert J. Polarization studies of Zr-based bulk metallic glasses for electrochemical machining. J Electrochem Soc 2014;161(4):E66–73.